

Membrane nanotubes physically connect T cells over long distances presenting a novel route for HIV-1 transmission

Stefanie Sowinski¹, Clare Jolly², Otto Berninghausen¹, Marco A. Purbhoo¹, Anne Chauveau¹, Karsten Köhler¹, Stephane Oddos¹, Philipp Eissmann¹, Frances M. Brodsky³, Colin Hopkins¹, Björn Önfelt⁴, Quentin Sattentau² and Daniel M. Davis^{1,5}

Transmission of HIV-1 via intercellular connections has been estimated as 100–1000 times more efficient than a cell-free process, perhaps in part explaining persistent viral spread in the presence of neutralizing antibodies^{1,2}. Such effective intercellular transfer of HIV-1 could occur through virological synapses^{3–5} or target-cell filopodia connected to infected cells⁶. Here we report that membrane nanotubes, formed when T cells make contact and subsequently part, provide a new route for HIV-1 transmission. Membrane nanotubes are known to connect various cell types, including neuronal and immune cells^{7–13}, and allow calcium-mediated signals to spread between connected myeloid cells⁹. However, T-cell nanotubes are distinct from open-ended membranous tethers between other cell types^{7,12}, as a dynamic junction persists within T-cell nanotubes or at their contact with cell bodies. We also report that an extracellular matrix scaffold allows T-cell nanotubes to adopt variably shaped contours. HIV-1 transfers to uninfected T cells through nanotubes in a receptor-dependent manner. These data lead us to propose that HIV-1 can spread using nanotubular connections formed by short-term intercellular unions in which T cells specialize.

To test for the presence of membranous connections, populations of T cells were labelled with the membrane dyes DiO (green) or DiD (red), mixed on fibronectin-coated coverslips and live cells were imaged by laser scanning confocal microscopy (LSCM). Differentially labelled T cells were readily observed connected by membranous tethers, confirming that cells were connected independently from tethers derived from cell division (Fig. 1a). Specifically, 16% of Jurkat T cells ($n > 500$) were connected after 16 h co-incubation. A small bias for cells with the same label being connected revealed that 3% were connected as a result

of cell division. Thus, 13% of Jurkat T cells were connected by tethers formed independently of cell division, and were therefore considered to be connected by membrane nanotubes.

T-cell nanotubes had an average length of $22 \pm 3 \mu\text{m}$, 5–10 times longer than filopodial bridges⁶, and could sometimes extend for over $100 \mu\text{m}$ (see Supplementary Information, Fig. S1). Reconstruction of three-dimensional fluorescence images confirmed that T-cell nanotubes were not tethered to the substratum and thus were distinct from filopodia¹⁴ (Fig. 1a and see Supplementary Information, Movie 1). Activated primary human or primary mouse T cells were similarly connected by nanotubes (see Supplementary Information, Fig. S1). Cells were generally connected by a single nanotube, although multiple (Fig. 1b) or branched nanotubes (see Supplementary Information, Fig. S1) could connect several T cells together.

T-cell nanotubes stained with fluorophore-conjugated phalloidin, indicating that they contained F-actin (Fig. 1c), consistent with the presence of F-actin within membrane nanotubes between other cell types^{7,11}. However, microtubules were not detected in T-cell nanotubes, which is in contrast with membrane nanotubes observed between macrophages, of which a subset of connections contain microtubules¹¹. Microtubules, and the characteristic midbody, were clearly observed within membranous tethers formed by cell division (Fig. 1d), further demonstrating that nanotubes are novel physical connections between T cells.

Time-lapse LSCM revealed that nanotubes between Jurkat T cells or activated primary T cells were formed by cells coming into contact and then moving apart (Fig. 1e and see Supplementary Information, Movies 2 and 3; $n > 120$). Importantly, transient contact between T cells does not inevitably lead to formation of a nanotube when cells part. Intercellular contacts that lasted less than approximately 2–3 min very rarely led to nanotube formation, whereas intercellular contacts

¹Division of Cell and Molecular Biology, Sir Alexander Fleming Building, Imperial College London, SW7 2AZ, UK. ²Sir William Dunn School of Pathology, University of Oxford, OX1 3RE, UK. ³The G. W. Hooper Foundation, Box 0552, 513 Parnassus Avenue, UCSF, San Francisco, CA 94143–0552, USA. ⁴Microbiology and Tumor Biology Center, Karolinska Institute, Box 280, S-171 77 Stockholm, Sweden.

⁵Correspondence should be addressed to D.M.D. (e-mail: d.davis@imperial.ac.uk)

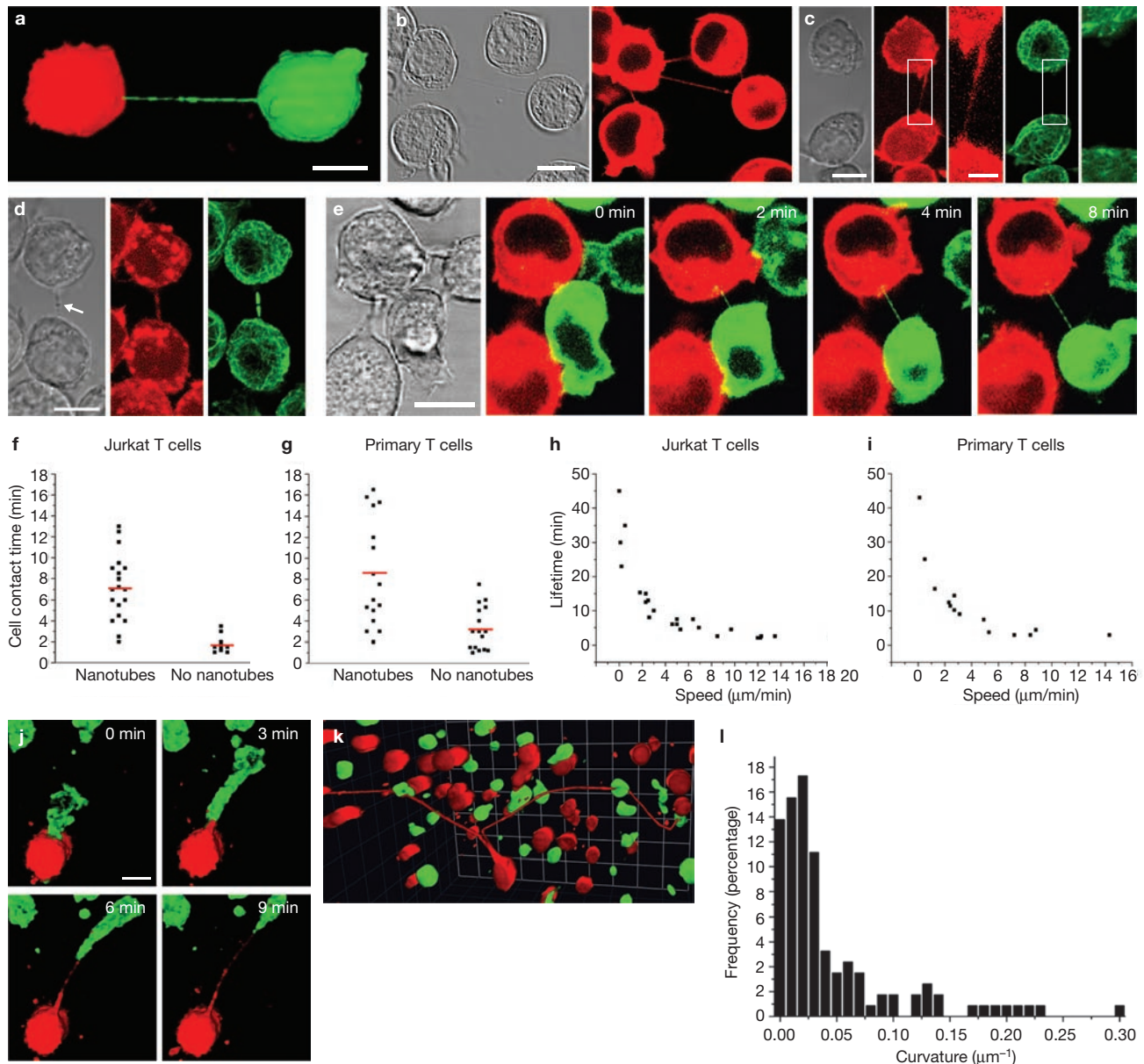


Figure 1 Membrane nanotubes connect human T cells. (a) Long membrane tethers, or membrane nanotubes, readily form between Jurkat T cells labelled with DiO (green) and DiD (red), $n > 500$. (b) Membrane nanotubes could occasionally network multiple cells, $n > 50$. (c) Jurkat T-cell cultures were fixed and stained for F-actin (red) and α -tubulin (green) revealing that membrane nanotubes contained F-actin but not microtubules, $n = 41$. Boxed regions are shown enlarged to better visualize the nanotube. (d) For comparison, cells connected by tethers derived from cytokinesis, containing a midbody (arrow), contained both F-actin and microtubules, $n = 21$. (e) Time-lapse microscopy reveals that membrane nanotubes form following intercellular contact ($n = 135$). (f, g) Time-lapse microscopy of Jurkat T cells (f, $n = 31$) and primary human T cells (g, $n = 32$) was analysed to record the length of time of contact between cells and then whether or not membrane nanotubes formed as cells departed. Contact between T cells led to nanotubes

sustained for > 4 min led to a significantly increased ($P < 0.01$) frequency of nanotube formation for both Jurkat (Fig. 1f) and primary human T cells (Fig. 1g). This indicates that a time-dependent process

generally only after cells had been in contact for > 4 min ($P < 0.01$, Mann-Whitney U). (h, i) Cell motility controls the lifetime of membrane nanotubes between Jurkat T cells (h, $n = 23$) and primary human T cells (i, $n = 14$). The combined speed of the two connected cells is plotted against the lifetime of the nanotube. (j) Time lapse microscopy of primary T cells labelled with DiO (green) and DiD (red) within a three-dimensional matrix reveals that nanotubes form after intercellular contact ($n = 5$), as observed in a two-dimensional culture. (k) Membrane nanotubes form between primary T cells in a three-dimensional extracellular matrix with any-shaped contour ($n = 114$; scale unit = $35 \mu\text{m}$). (l) Distribution of nanotube curvatures ($n = 114$) were calculated as the inverse of the radius of a fitted circle. A curvature of zero represents a straight nanotube. Repeated measurements on the same nanotube indicated that the error in each datapoint was $0.01 \mu\text{m}^{-1}$. Scale bars represent $10 \mu\text{m}$ in a–e and j. The scale bar in the inset of e represents $3 \mu\text{m}$.

is required for the formation of T-cell nanotubes. Once formed, both Jurkat (Fig. 1h) and primary human T cells (Fig. 1i) remained connected by nanotubes for prolonged periods of time, dependent on the

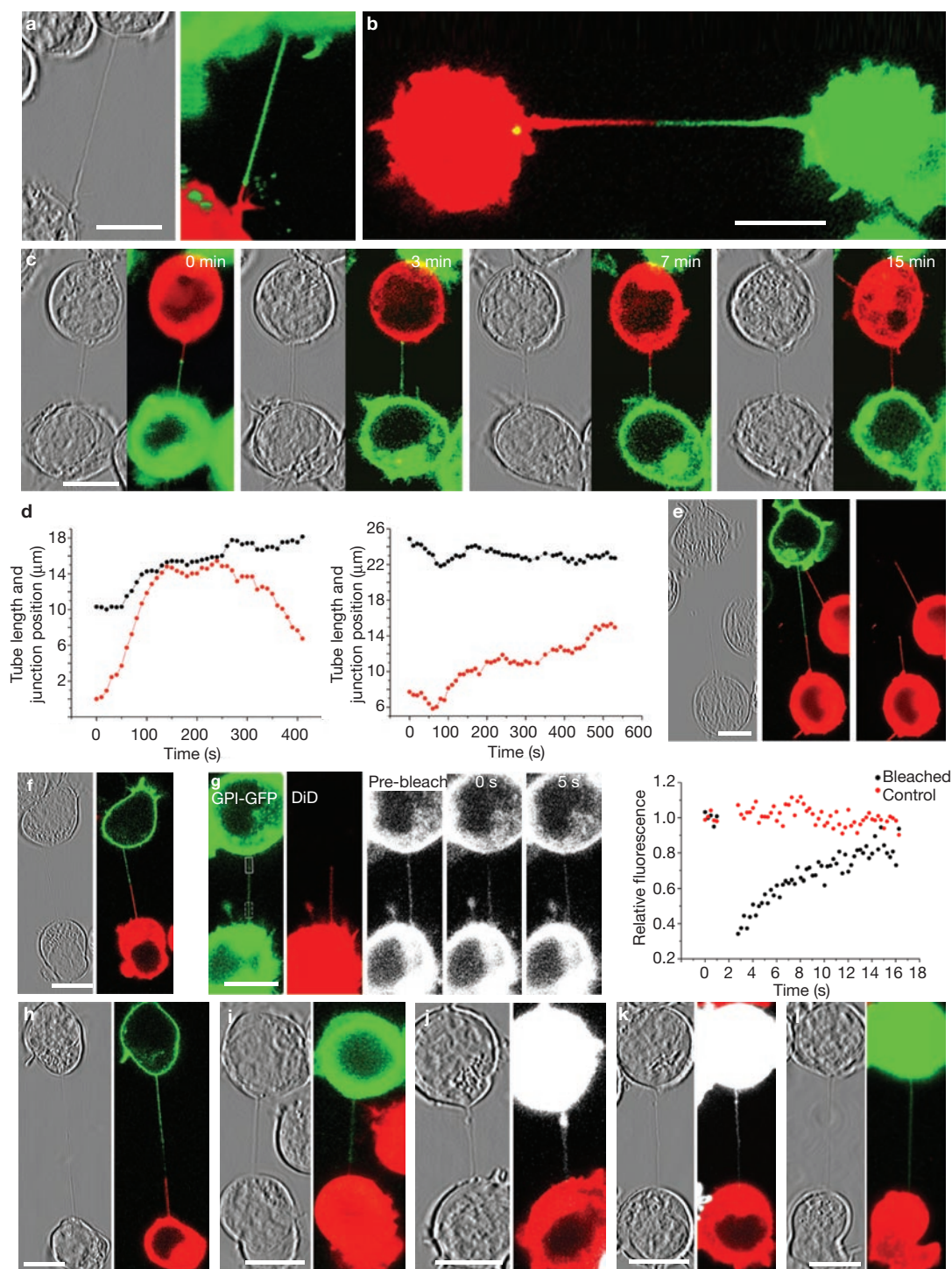


Figure 2 T-cell nanotubes are not open-ended tunnels and contain a junction. (a, b) Jurkat T cell (a) and primary human T-cell (b) nanotubes contain a junction revealed by a distinct border between DiO (green) and DiD (red) membrane dyes ($n = 151$). (c) Time-lapse imaging of two differently labelled cells connected by a nanotube demonstrates dynamic movement of the junction ($n = 15$). (d) Position of the junction within the nanotube (black dots) and length of the nanotube (red dots) are plotted against time. (e, f) Proteins anchored to the outer or inner leaflet of the cell surface can access T-cell nanotubes. DiD-labelled (red) cells mixed with cells expressing GPI-GFP (e, $n = 25$; red channel is also shown separately to clearly show junction) or palmitoylated YFP (f, both green; $n = 23$) are shown. (g) Movement of GPI-anchored GFP along Jurkat T-cell nanotubes was assessed by FRAP. Micrographs show GPI-GFP fluorescence (green)

bleached along 3 μm of nanotube on one side of the junction, as determined by one of the cells being stained with membrane dye DiD (red). GFP fluorescence of nanotube is shown pre-bleaching, immediately after bleaching and then 5 s later. The graph includes datapoints from four different nanotubes (representative of 10), showing fluorescence of the bleached region on one side of the nanotube junction (black dots) and the fluorescence of a 'control' unbleached 3 μm section on the other side of the nanotube junction (red dots). (h, i) Transmembrane protein ICAM-1 (h) or class I MHC protein HLA-Cw7 (i), each tagged with intracellular GFP, can access T-cell nanotubes ($n = 28$ and 15 respectively). (j-l) Cytoplasmic proteins and dyes can access T-cell nanotubes. Fluorescence micrographs of cytoplasmic GFP (j, $n = 19$; white), cytoplasmic CFDA (k, $n = 12$; white) and calcein (l, $n = 12$; green). The scale bars represent 10 μm .

motility of the connected cells. Lymph-node cells readily sustain intercellular contacts for several minutes and move with an average speed of approximately $2\text{--}10\ \mu\text{m}\ \text{min}^{-1}$ depending on the stage of immune response^{15,16}, which are suitable conditions for membrane nanotubes to form and persist *in vivo*.

A major difference between cell migration in tissue and on fibronectin-coated coverslips is that the former provides for three-dimensional cell migration, which is known to significantly alter the dynamics of intercellular contacts¹⁷. Thus, we next examined whether nanotubes between primary human T cells could form within a three-dimensional mimic of extracellular matrix. T-cell nanotubes readily formed after intercellular contact (Fig. 1j). Nanotubes in this environment had an average length of $38.4 \pm 7.6\ \mu\text{m}$ (but could extend $> 200\ \mu\text{m}$) and could readily persist for $> 30\ \text{min}$, similar to the properties of T-cell nanotubes in a two-dimensional environment. However, one dramatic distinction was that the three-dimensional matrix supported nanotubes to adopt curved morphologies (Fig. 1k, l), allowing nanotubes to connect T cells over long distances even when a direct path is obstructed.

Previous studies indicated that membrane between PC12 cells was seamlessly connected through nanotubes⁷. In striking contrast, membrane marked with different fluorophores from each connected T cell defined a specific junction (Fig. 2a, b). Thus, although it remains possible that small amounts of membrane dye could transfer between T cells through nanotubes, it is clear that membrane does not seamlessly mix along the length of a T-cell nanotube. The junction was highly motile and able to move bidirectionally along the length of the nanotube with an average speed of $0.05 \pm 0.01\ \mu\text{m}\ \text{s}^{-1}$ (Fig. 2c and see Supplementary Information, Movie 4). Analysis confirmed that the junction within a nanotube generally moves independently from stretching or contraction of the nanotube itself (Fig. 2d).

Both glycosylphosphatidylinositol (GPI)-anchored and palmitoylated fluorescent proteins were observed along T-cell nanotubes, indicating that proteins anchored to either the outer or inner leaflet of the lipid bilayer have access (Fig. 2e, f). Rates of fluorescence recovery after photobleaching (FRAP) were the same order of magnitude for a membrane-anchored protein in T-cell nanotubes ($t_{1/2} = 4.0 \pm 0.9\ \text{s}$ for a bleached region of $3\ \mu\text{m}$ diameter, $n = 10$; Fig. 2g) as for at the cell surface ($t_{1/2} = 5.4 \pm 0.5\ \text{s}$, $n = 7$; data not shown). Geometrical considerations predict slightly faster diffusion of proteins within nanotubes compared with the cell surface, but these effects are likely to be beyond the limit of detection here¹⁸. Large transmembrane proteins, such as GFP-tagged ICAM-1 (Fig. 2h) or GFP-tagged HLA-Cw7, a class I MHC protein endogenously expressed by Jurkat T cells (Fig. 2i), could also readily access T-cell nanotubes. Importantly, these proteins did not seamlessly traffic between connected cells and a junction within the nanotube was commonly observed (for examples, see Fig. 2e, f, h, i). Cytosolic GFP (Fig. 2j), or the small cytoplasmic dyes CFDA and calcein (Fig. 2k, l), could also enter T-cell nanotubes, but similarly did not flow seamlessly between connected cells. Thus, T-cell nanotubes are not open-ended tunnels and do not allow simple exchange of membrane or cytosol between cells by diffusion.

To probe their structure at higher resolution, nanotubes were identified between T cells labelled with membrane dyes using LSCM, and the same cells were then resin embedded and cut into a series of $60\ \text{nm}$ slices for transmission electron microscopy (TEM). Two nanotubes are shown

in Fig. 3 with a diameter of $180\text{--}380\ \text{nm}$, considerably thicker than non-biological membrane tethers pulled from vesicles¹⁹ or dynamin-coated membrane tubules²⁰. Intriguingly, multiple membrane-delimited compartments lie within nanotubes (Fig. 3b' and d').

Where a junction was visible in the nanotube by light microscopy (Fig. 3a), electron micrographs revealed a discrete connection, where the ends of two membranous extensions meet, partly in parallel (Fig. 3b'' and see Supplementary Information, Movie 5). As T cells have a significant excess of cell membrane stored in ruffles (as revealed by osmotically induced swelling, for example), it seems feasible that such membrane extensions could be readily pulled out from each cell when cells move apart from each other. In other cases, where the nanotube membrane seemed to be derived solely from one of the connected cells (for example see Fig. 1a), TEM revealed that the tip of the nanotube protruded into the surface membrane of the other connected cell interacting with a coated pit (Fig. 3c, d and see Supplementary Information, Movie 6). Thus, these high resolution images further demonstrate that T-cell nanotubes are not open-ended tunnels. Also, they confirm that the ultrastructure of T-cell nanotubes is entirely distinct from membranous tethers derived from T-cell division, which contain a characteristic midbody (Fig. 3e).

As some electron micrographs indicated that nanotubes can interact with coated pits (Fig. 3d), we examined whether clathrin-mediated processes were involved in nanotube formation. Small interference RNA (siRNA)-mediated knockdown of clathrin heavy chain in Jurkat T cells was dramatic and caused a functional impairment in that cells were far less efficient at internalizing fluorescent transferrin. However, there was no discernible effect of clathrin knockdown on the frequency or length of nanotubes, or on the time of cell contact needed to form nanotubes (see Supplementary Information, Fig. S2).

At present, the clearest indication of a role for membrane nanotubes in immune-cell communication is transmission of calcium-mediated signals between distant myeloid cells⁹. Thus, we examined whether calcium-mediated signals could traffic through T-cell nanotubes. Two populations of Jurkat cells, one transfected to express GPI-GFP, were co-cultured for 1 h to allow nanotube formation before being loaded with a calcium indicator. For cells connected by a tether derived from cell division, containing the characteristic midbody, a calcium flux induced in one cell by mechanical stimulation could transfer to the connected cell in approximately 50% of tests (Fig. 3f). However, a calcium flux never transferred between T cells connected by a membrane nanotube (Fig. 3g). This is in striking contrast to the functional properties of membrane nanotubes between myeloid cells⁹ and demonstrates that membrane nanotubes have distinct structures and/or functions in different cell types. Thus, other functional consequences of T-cell nanotubes were examined.

Membrane nanotubes readily formed after intercellular contact between cells infected with the LAI strain of HIV-1 (Jurkat_{LAI}) and uninfected Jurkat T cells (Fig. 4a) and HIV-1 infection did not alter the frequency of nanotube formation (Fig. 4b). We next stained for the presence of HIV-1 Env and capsid protein Gag in nanotubes connecting uninfected and infected cells. Jurkat_{LAI} were co-incubated with uninfected Jurkat labelled with a cytoplasmic dye (Fig. 4c) or uninfected primary CD4⁺ T cells labelled with a non-blocking CD4 monoclonal antibody (mAb; Fig. 4d). After 1 h of coculture, colocalized Gag and Env labelling was frequently detected on membrane nanotubes connecting HIV-1-infected to uninfected T cells (Fig. 4c, d). The observation of colocalized Env and Gag proteins at the plasma membrane is consistent with the presence of

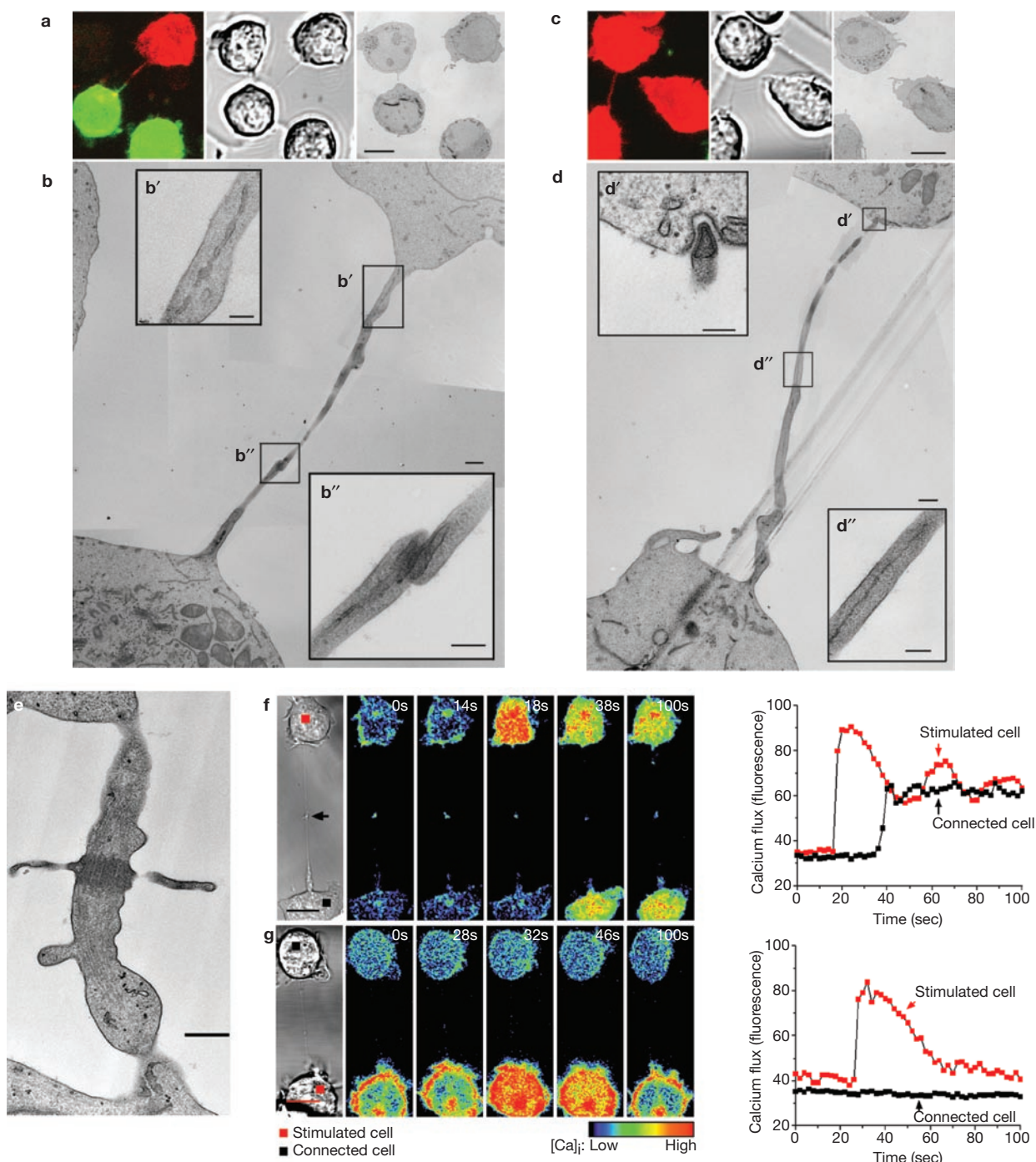


Figure 3 The ultrastructure of T-cell nanotubes reveals a novel class of membranous connection between cells. (a–d) T-cell nanotubes were identified by light microscopy and then visualized by TEM. High resolution images (b, d) of the full length of the nanotubes shown in a and c were reconstructed from images of 13 individual 60 nm epon sections. Individual sections can be seen in Supplementary Information, Movies 5 and 6, respectively. The junction between membrane dyes within a nanotube corresponded to a discrete connection formed between individual cellular protrusions, as visualized by TEM (a, b). Inserts show higher magnifications of the nanotube and the junction. Where light microscopy indicated that the nanotube was derived solely from membrane of one connected cell, TEM revealed that the nanotube protruded into an invagination of the other connected cell (c, d). (e) For comparison, TEM of an intercellular membrane connection derived from cytokinesis revealed the characteristic dense microtubule bundles of the midbody. (f, g) Membrane nanotubes do not facilitate intercellular

calcium signalling amongst T cells. Intercellular calcium signalling was compared in T cells connected via (f) tethers derived from cell division or (g) membrane nanotubes. Tethers derived from cell division were identified as connections between cells of the same type (that is, both untransfected Jurkat T cells or both Jurkat T cells expressing GPI–GFP) and containing the characteristic midbody (arrow) (f). Membrane nanotubes (g) were identified as connections between Jurkat T cells and GPI–GFP-expressing Jurkat T cells. An intracellular calcium flux was induced within one cell of each pair (red square) by mechanical stimulation using a microinjector needle. Graphs show the extent of calcium flux within the stimulated (red squares) and connected cells (black squares). Intercellular calcium fluxes amongst T cells connected by tethers derived from cell division were detected in 19 of 37 cases, whereas intercellular calcium signalling was never detected between nanotube connected T cells ($n = 35$). The scale bars represent 10 μm in a, c, f and g, 500 nm in b, d and e, and 200 nm in b', b'', d' and d''.

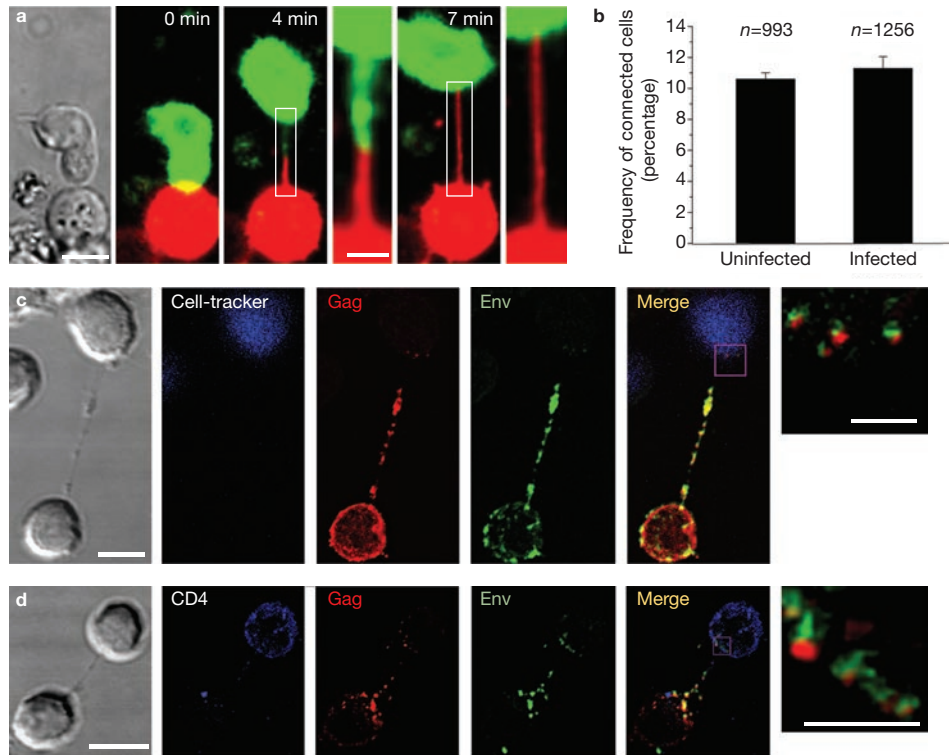


Figure 4 Membrane nanotubes present a novel route for HIV-1 to spread between T cells. **(a)** Membrane nanotubes were formed after intercellular contact between Jurkat_{LAI} T cells (labelled with DiD; red) and uninfected Jurkat T cells (labelled with DiO; green; $n = 8$). Boxed regions are shown enlarged to better visualize the nanotube. **(b)** The frequency of membrane nanotubes formed between uninfected Jurkat T cells and Jurkat_{LAI} T cells or between two populations of uninfected Jurkat T cells is shown after 1.5–2 h co-incubation (n , number of cells counted over three

independent experiments; difference between infected and uninfected cells n.s.). **(c, d)** Jurkat_{LAI} T cells were cocultured with uninfected Jurkat T cells, stained with CellTracker **(c)**, blue, $n = 62$) or uninfected CD4⁺ primary cells, stained for CD4 **(d)**, blue, $n = 6$). HIV-1 Env (green) and Gag (red), colocalized (yellow), in nanotubes connecting Jurkat_{LAI} T cells to previously uninfected T cells. Boxed regions are enlarged to show HIV-1 Env and Gag associated with the previously uninfected T cell. Scale bars represent 10 μm . Scale bars in enlarged regions represent 3 μm .

late-stage virus^{21,22}. Where HIV-1 antigens were associated with nanotubes, viral proteins were readily detected in the previously uninfected target cell. In contrast, neither Gag nor Env were detected in uninfected CD4⁺ T cells that were not physically connected to infected cells. These data imply that 1 h of co-incubation is not enough time to allow significant spread of HIV-1 by cell-free virions, and that intercellular transmission of HIV-1 through nanotubes is considerably more efficient.

To directly determine whether HIV-1 can move between T cells through nanotubes, LSCM of live HIV-1 in T cell cultures was performed using Jurkat T cells infected with a recombinant HIV-1 in which GFP had been fused with the Gag open reading frame to express Gag–GFP²³. Puncta of Gag–GFP moved along nanotubes from infected towards uninfected cells (Fig. 5a, b and see Supplementary Information, Movie 7). Micrographs suggest that Gag–GFP entered the target cell contacted by the nanotube (Fig. 5b and see Supplementary Information, Movie 8).

Gag–GFP moved along T-cell nanotubes with an average speed of $0.08 \pm 0.03 \mu\text{m s}^{-1}$ (Fig. 5c). This is of the same order of magnitude as actin-driven movement of ‘nodules’ along retractile fibres^{24,25} and approximately 2–5 times faster than the movement of murine leukaemia virus along filopodial connections between cells^{6,26}. Thus, T-cell nanotubes could mediate a novel mechanism for rapid, long-distance intercellular transmission of HIV-1. This mode of viral spread might, for example, have particular relevance to the fast and massive infection

of CD4⁺ T cells observed in secondary lymphoid tissue during acute HIV-1 and SIV infection^{27,28}. To determine how important intercellular connections are for HIV-1 transmission, transfer of Gag from Jurkat_{LAI} to uninfected Jurkat cells was compared in conditions that do or do not allow intercellular connections. Transfer of Gag was almost completely abrogated when cells were shaken to break intercellular connections (Fig. 5d) or when cells were separated by a Transwell membrane (Fig. 5e). These data are in close agreement with previous studies² and imply that contact-dependent mechanisms are central to HIV-1 dissemination.

To determine whether entry of HIV-1 into cells through nanotubes is receptor-dependent, Jurkat_{LAI} and uninfected Jurkat cells were co-incubated in the presence of blocking mAb against CD4 or the gp120 subunit of Env. Blocking CD4 or Env did not alter the frequency of nanotube formation (see Supplementary Information, Fig. S3), consistent with membrane nanotubes being distinct from filopodial bridges that are stabilized by Env⁶. Blocking CD4 or Env did not alter the high frequency of Gag observed in nanotubes, but almost completely prevented Gag reaching the uninfected target cells (Fig. 5f, $P < 0.05$ or 0.01 , respectively). Next, transfer of Gag from Jurkat_{LAI} to the human CD4-deficient T-cell line A2.01 and its parental CD4-positive line A3.01 was examined. The frequency of Gag associated with nanotubes connecting Jurkat_{LAI} to either A2.01 or A3.01 was not statistically different ($P > 0.05$). However, there was a dramatic difference in Gag transfer to A3.01 or A2.01 ($P < 0.001$). Indeed, Gag did

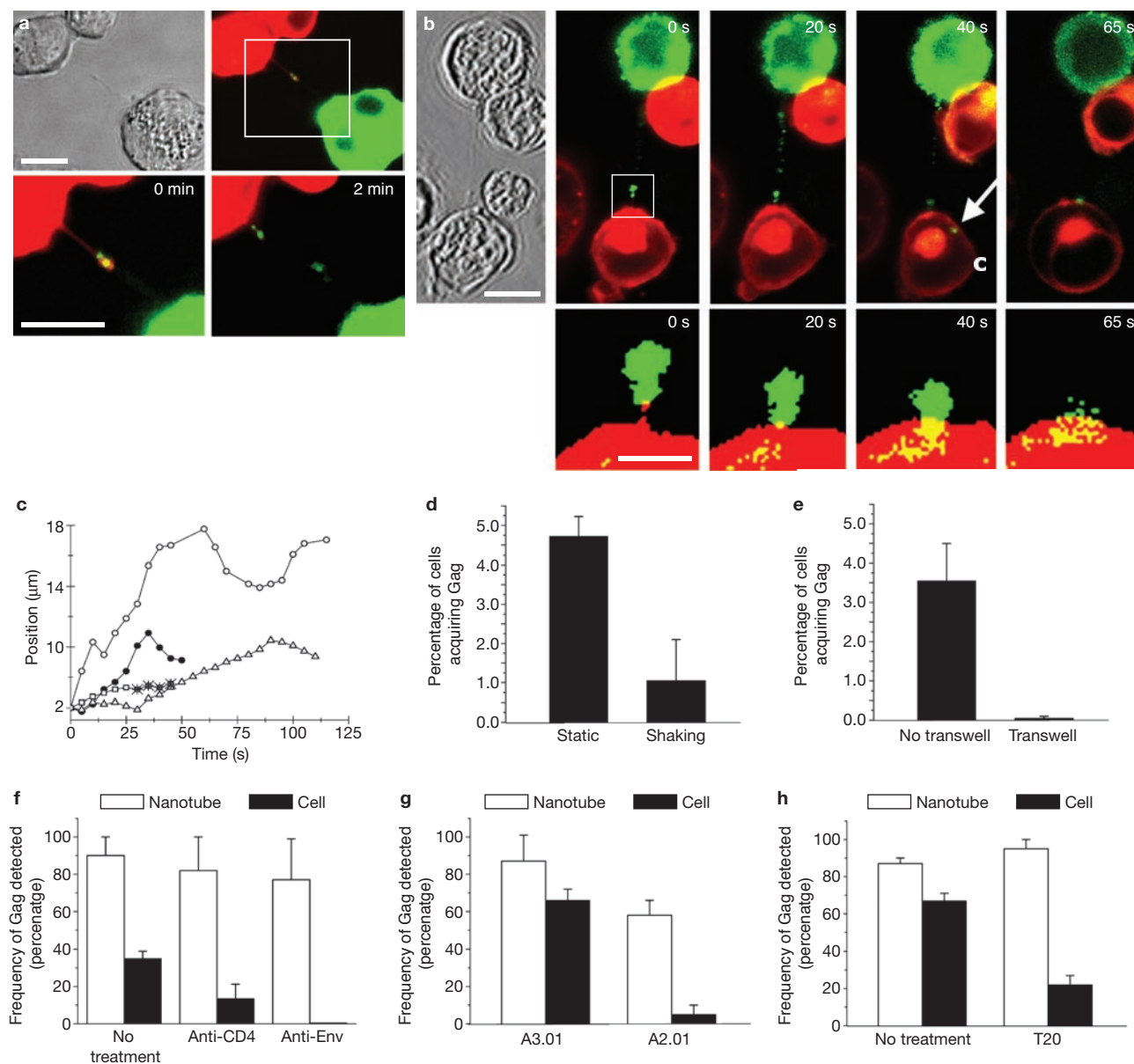


Figure 5 HIV-1 spread via membrane nanotubes is receptor dependent. (a, b) Time-lapse imaging of Gag-GFP (green), expressed in the context of the fully infectious virus, along a membrane nanotube connecting infected with uninfected Jurkat T cells (stained with membrane dye DiI; red; $n = 8$). Boxed region in a is shown enlarged, at two time-points, to visualize movement of Gag-GFP along the nanotube. Boxed regions in b are shown enlarged, indicating that the Gag-GFP reaches the initially uninfected T cell. Enlarged images in b are shown with a particularly high contrast, compensating for significant bleaching that occurred in all time-lapse imaging of Gag-GFP. The arrow indicates Gag-GFP within the cytoplasm of the initially uninfected T cell. (c) The position of Gag-GFP is plotted against time showing generally directed movement from uninfected to infected cells. (d, e) The efficiency of Gag transfer from Jurkat_{LAI} T cells to uninfected Jurkat T cells was compared

not transfer to A2.01 cells to any significant level (Fig. 5g). Similarly, the peptide inhibitor T20 abrogated transmission of Gag to uninfected cells (Fig. 5h; $P < 0.01$). These data confirm that intercellular spread of HIV-1 through T-cell nanotubes is receptor dependent, consistent with the structure of T-cell nanotubes preventing a seamless connection of membrane or cytoplasm (Figs 2, 3).

when cells were co-incubated for 5 h, and kept static or continuously shaken to disturb any intercellular connections (d), or were separated by a Transwell membrane (e). (f-h) Nanotubes connecting infected as well as the uninfected T cells and the uninfected target cells (white and black bars, respectively), were scored as to whether or not Gag could be detected (f). Jurkat_{LAI} T cells were cocultured with uninfected Jurkat T cells in the presence of blocking mAb against CD4 or the gp120 subunit of Env (n , total number of nanotubes scored = 81); (g). Jurkat_{LAI} T cells were cocultured with the human CD4-deficient T cell line A2.01 or its parental CD4-positive line A3.01 (n , total number of nanotubes scored = 36). (h) Jurkat_{LAI} T cells were cocultured with uninfected Jurkat T cells with or without the fusion inhibitor T20 (n , total number of nanotubes scored = 44). Data are representative of two independent experiments in d-h. The scale bars represent 10 μm in a and b.

It is an emerging theme that mammalian viruses commonly exploit cell membrane protrusions for intercellular dispersal. Pseudo-rabies virus capsids are transferred from cellular projections into uninfected cells²⁹, vesicular clusters containing a structural protein of herpes simplex virus are transported within long membrane protrusions towards adjacent cells³⁰, and murine leukaemia virus moves along the surface of

filopodia before viral entry at the cell body of fibroblasts^{6,26}. Transmission of viruses in this manner can circumvent the rate-limiting step of diffusion between cells, and may minimize exposure of the virus to extracellular antibodies or complement.

In summary, our data show that T-cell nanotubes are novel physical connections between T cells that can have important consequences for allowing rapid spread of HIV-1. As the ability of HIV-1 to spread between cells is a major determinant of its virulence, this mechanism of HIV-1 transmission could be important to its pathogenicity and may open new avenues for drug targets. □

METHODS

Cells. The CD4⁺-CXCR4⁺ T cell line Jurkat CE6.1 (from the American Type Culture Collection; ATCC) was cultured in RPMI 1640 supplemented with 10% FCS, 2 mM L-glutamine, 1 mM sodium pyruvate, 1× non-essential amino acids, 50 U ml⁻¹ penicillin and 50 µg ml⁻¹ streptomycin (Invitrogen). Jurkat T cells were nucleofected or electroporated (Amaxa or Microporator, Digital Bio) with pcDNA3.1-GPI-GFP, pcDNA3.1-ICAM-1-EGFP (gift from J. Millan and F. Sanchez-Madrid, Universidad Autonoma di Madrid, Spain), pcDNA3.1-HLA-Cw7-GFP, pEGFP-C2 (Clontech) or pEYFP-Mem (Clontech). CD4⁺ A2.01 and its CD4⁺ parental line A3.01 (Center for AIDS Research, CFAR, New York, NY) were cultured as for Jurkat cells.

Jurkat cells were infected with the CXCR4-tropic HIV-1 strain (referred to as Jurkat_{LAI}), infection being monitored by flow cytometry, as previously described³.

Primary CD4⁺ T cells were purified from human peripheral blood by density gradient centrifugation (Ficoll-Paque Plus; Amersham Biosciences) followed by negative immunomagnetic selection (StemCell). Flow cytometry revealed 98% of cells were CD4⁺CD3⁺. Where indicated, CD4⁺ T cells cultured in DMEM supplemented with 10% human serum (type AB; Sigma-Aldrich), 30% nutrient mixture F-12 (Ham), 2 mM L-glutamine, 1 mM sodium pyruvate, 1× non-essential amino acids, 50 U ml⁻¹ penicillin, 50 µg ml⁻¹ streptomycin, 50 µM 2-mercaptoethanol (all purchased from Invitrogen) were activated with 500 ng ml⁻¹ ionomycin (Sigma) and 50 ng ml⁻¹ phorbol 12-myristate 13-acetate (PMA; Sigma) for 2 days before imaging. For longer-term culture, T cells were first activated with ionomycin and PMA and then cultured in DMEM-based medium containing 20 U ml⁻¹ rIL-2 (Roche).

To test the efficiency of Gag transfer, 1 × 10⁶ CFSE-labelled Jurkat and Jurkat_{LAI} cells were coincubated on fibronectin-coated surfaces for 5 h at 37 °C, and kept either static or with gentle shaking². Alternatively, 2 × 10⁵ CFSE-labelled Jurkat cells and Jurkat_{LAI} cells were coincubated together or separately across a Transwell membrane (3 µm-pore; Nunc). Cells were harvested, fixed, permeabilized, stained for Gag and analysed by flow cytometry.

Cytoplasmic and membrane dyes. T cells were labelled with 25 µM carboxyfluorescein diacetate succinimidyl ester (CFDA), 1–2.5 µM 1,1'-dioctadecyl-3,3,3',3'-tetramethylindodicarbocyanine perchlorate (DiD) or 3,3'-dioctadecyloxycarbocyanine perchlorate (DiO), 10 µM CellTracker Green, or 8 µM calcein AM in 0.02% Pluronic F-127 (all purchased from Molecular Probes).

Live-cell imaging. Cells were imaged in eight-well chambered coverglasses (Lab-Tek Chambered Borosilicate Coverglass) pre-coated with 10 µg ml⁻¹ fibronectin (Sigma). Cells were imaged at 37 °C, 5% CO₂ by resonance scanning LSCM (TCS SP5 RS; Leica) using excitation wavelengths of 488 and 568 or 633 nm and a 63× water immersion objective (NA = 1.2). Image analysis was performed using Velocity (Improvision) or Image J (NIH, Bethesda, MA). Brightness and contrast were changed in some images and some brightfield images were 'embossed' (Adobe Photoshop), only to increase visibility of nanotubes.

For FRAP measurements, GPI-GFP was bleached in 3 µm regions of nanotubes or plasma membrane. The recovery half-life was determined by an exponential fit of the bleach region fluorescence, corrected for imaging-related bleaching (Originlab).

For imaging calcium fluxes, 1 × 10⁵ Jurkat were mixed with 1 × 10⁵ Jurkat transfectants expressing GPI-GFP and plated onto coverslip-bottomed 50 mm dishes (MatTek) pre-coated with 10 µg ml⁻¹ fibronectin (Sigma). Cells were incubated for 1 h at 37 °C, 5% CO₂, to allow formation of membrane nanotubes, loaded for

30 min at room temperature with 5 µg ml⁻¹ fluo-4 AM (Invitrogen), washed and imaged by LSCM. Intracellular calcium fluxes were induced by physical stimulation with a 4 µm-tipped micromanipulator (Eppendorf).

For imaging in a three-dimensional matrix, 1 × 10⁵ primary T cells labelled with DiO were mixed with 1 × 10⁵ primary T cells labelled with DiD in Matrigel basement-membrane matrix (BD Bioscience, Bedford, MA) diluted 1:4 with cell culture media and imaged at 37 °C, 5% CO₂ by resonance scanning LSCM using a 20× dry objective (NA = 0.5). The radius of a circle fitted to each T-cell nanotube was determined using MatLab (The MathWorks).

Infectious HIV-1-GFP was prepared by cotransfecting 293T cells with 1 µg pNL4-3^{EGFP} (gift from H.-G. Kräusslich, University of Heidelberg, Heidelberg, Germany) and 1 µg pNL4-3 (ref. 23). Supernatants were collected 48 h post-transfection, filtered, and HIV-1-GFP was stored at -150 °C. Jurkat cells (2.5–5 × 10⁶) were infected with undiluted HIV-1-GFP and confirmed to express Gag-GFP²³. Four days post-infection, infected Jurkat cells were washed, resuspended in RPMI 1640 with 10% FCS, and mixed with an equal number of uninfected DiD-labelled Jurkat cells. Cells were incubated for at least 1 h on fibronectin-coated chambered coverglass (LabTek) and imaged at 37 °C, 5% CO₂ (LSM 5 Pascal; Zeiss).

Fixation and immunostaining of Jurkat cells. Jurkat T cells were fixed with 0.1% glutaraldehyde, 2% formaldehyde in PBS for 1 min at room temperature followed by Cytotfix-Cytoperm (BD Bioscience) for 5 min at 37 °C and quenched using 50 mM NH₄Cl, 20 mM glycine. Cells were stained at 4 °C for 45 min with anti-α-tubulin mAb (Clone DM 1A, Sigma) followed by Alexa-488 goat anti-mouse antibody (Molecular Probes). F-actin was labelled with Alexa-633 phalloidin (Molecular Probes).

Jurkat_{LAI} T cells were washed, mixed with an equal number of dye-labelled uninfected Jurkat T cells or primary CD4⁺ T cells and incubated for 1 h at 37 °C in the presence of the non-blocking gp41-specific mAb 50-69 (CFAR)³ and the non-blocking anti-CD4 mAb L120 (CFAR)³. Cells were fixed in 4% formaldehyde, 1% BSA in PBS for 15 min, permeabilized and stained with rabbit antisera against HIV Gag⁶¹⁷ and Gag⁶²⁴ (CFAR)³.

For blocking experiments, 2.5 × 10⁵ Jurkat_{LAI} cells were mixed with an equal number of uninfected Jurkat cells and incubated on fibronectin coated coverslips for 1.5 h at 37 °C either untreated or in the presence of the following mAbs that inhibit CD4-gp120 binding; CD4-specific mAbs Q4120 (CFAR) and 13B8 (CFAR), or the HIV-1 gp120-specific mAbs b12 and 2G12 (CFAR and Polymun Scientific, respectively). Alternatively, 1.25 × 10⁵ Jurkat_{LAI} were mixed with uninfected Jurkat cells in the presence or absence of 10 µg ml⁻¹ of the HIV-1 fusion inhibitor T20 (NIH). Additionally, 1.25 × 10⁵ Jurkat_{LAI} were incubated with A3.01 (CD4⁺) or A2.01 (CD4⁻) T cells as described above. Cells were then fixed, stained for HIV-1 Gag and imaged by LSCM (TCS SP2/5 RS, Leica or Radiance 2000 MP, Bio-Rad).

Electron microscopy. Jurkat cells, seeded on Cellocate glass-gridded coverslips (Eppendorf), were fixed in formaldehyde-glutaraldehyde and treated with 1% reduced osmium followed by 1% tannic acid. Samples were processed for en-face embedding in epon and only grid areas containing cells with nanotubes were cut. Serial ultrathin 60-nm sections were stained with lead citrate and observed with a transmission electron microscope (Philips CM12; FEI UK). Cells connected with nanotubes were identified by aligning electron micrographs with brightfield images of the same area.

Clathrin knockdown. Jurkat cell (1.6 × 10⁶) were transfected with 8 µg siRNA against clathrin heavy chain ((AA)GCAATGAGCTGTTTGAAGA, as used previously²¹) or a control siRNA ((AA)TTCTCCGAACGTGTACAGT; Qiagen) by electroporation (Microporator; Digital Bio). After 3 days, the extent of knockdown was assayed by western blotting with anti-clathrin heavy chain mAb TD.1 (Covance) and by the extent of uptake of Alexa-488 transferrin (Molecular Probes) while, in parallel, cells were assayed for membrane nanotube formation.

Statistical analysis. ANOVA or Mann-Whitney U was used as a statistical test for all data and error bars are shown as s.e.m., unless stated otherwise.

Note: Supplementary Information is available on the Nature Cell Biology website.

ACKNOWLEDGMENTS

We thank M. A. A. Neil, P. M. W. French, N. J. Burroughs, E. Vivier and members of our laboratories for useful discussions. This research was funded by The

Biotechnology and Biological Sciences Research Council, a Wellcome Trust studentship (to S.S.), The Medical Research Council, grant P01-AI064520 from the National Institutes of Health and a Lister Institute Research Prize.

AUTHOR CONTRIBUTIONS

S.S., C.J., O.B., M.A.P., A.C., K.K. and P.E. designed and performed experiments. S.O. and B.Ö. helped analyse data. F.B., C.H., B.Ö., Q.S. and D.M.D. helped design experiments. D.M.D. conceived the project and wrote the paper with S.S. and important input from all co-authors.

COMPETING FINANCIAL INTERESTS

The authors declare no competing financial interests.

Published online at <http://www.nature.com/naturecellbiology/>

Reprints and permissions information is available online at <http://npg.nature.com/reprints-and-permissions/>

- Dimitrov, D. S. *et al.* Quantitation of human immunodeficiency virus type 1 infection kinetics. *J. Virol.* **67**, 2182–2190 (1993).
- Sourisseau, M., Sol-Foulon, N., Porrot, F., Blanchet, F. & Schwartz, O. Inefficient human immunodeficiency virus replication in mobile lymphocytes. *J. Virol.* **81**, 1000–1012 (2007).
- Jolly, C., Kashafi, K., Hollinshead, M. & Sattentau, Q. J. HIV-1 cell to cell transfer across an Env-induced, actin-dependent synapse. *J. Exp. Med.* **199**, 283–293 (2004).
- Sol-Foulon, N. *et al.* ZAP-70 kinase regulates HIV cell-to-cell spread and virological synapse formation. *EMBO J.* **26**, 516–526 (2007).
- McDonald, D. *et al.* Recruitment of HIV and its receptors to dendritic cell-T cell junctions. *Science* **300**, 1295–1297 (2003).
- Sherer, N. M. *et al.* Retroviruses can establish filopodial bridges for efficient cell-to-cell transmission. *Nature Cell Biol.* **9**, 310–315 (2007).
- Rustom, A., Saffrich, R., Markovic, I., Walther, P. & Gerdes, H. H. Nanotubular highways for intercellular organelle transport. *Science* **303**, 1007–1010 (2004).
- Onfelt, B., Nedvetzki, S., Yanagi, K. & Davis, D. M. Cutting edge: Membrane nanotubes connect immune cells. *J. Immunol.* **173**, 1511–1513 (2004).
- Watkins, S. C. & Salter, R. D. Functional connectivity between immune cells mediated by tunneling nanotubes. *Immunity* **23**, 309–318 (2005).
- Stinchcombe, J. C., Bossi, G., Booth, S. & Griffiths, G. M. The immunological synapse of CTL contains a secretory domain and membrane bridges. *Immunity* **15**, 751–761 (2001).
- Onfelt, B. *et al.* Structurally distinct membrane nanotubes between human macrophages support long-distance vesicular traffic or surfing of bacteria. *J. Immunol.* **177**, 8476–8483 (2006).
- Gerdes, H. H., Bukoreshtliev, N. V. & Barroso, J. F. Tunneling nanotubes: a new route for the exchange of components between animal cells. *FEBS Lett.* **581**, 2194–2201 (2007).
- Davis, D. M. Intercellular transfer of cell-surface proteins is common and can affect many stages of an immune response. *Nature Rev. Immunol.* **7**, 238–243 (2007).
- Faix, J. & Rottner, K. The making of filopodia. *Curr. Opin. Cell Biol.* **18**, 18–25 (2006).
- Miller, M. J., Safrina, O., Parker, I. & Cahalan, M. D. Imaging the single cell dynamics of CD4+ T cell activation by dendritic cells in lymph nodes. *J. Exp. Med.* **200**, 847–856 (2004).
- Allen, C. D., Okada, T., Tang, H. L. & Cyster, J. G. Imaging of germinal center selection events during affinity maturation. *Science* **315**, 528–531 (2007).
- Gunzer, M. *et al.* Antigen presentation in extracellular matrix: interactions of T cells with dendritic cells are dynamic, short lived, and sequential. *Immunity* **13**, 323–332 (2000).
- Daniels, D. R. & Turner, M. S. Diffusion on membrane tubes: a highly discriminatory test of the Saffman-Delbruck theory. *Langmuir* **23**, 6667–6670 (2007).
- Roux, A. *et al.* Role of curvature and phase transition in lipid sorting and fission of membrane tubules. *EMBO J.* **24**, 1537–1545 (2005).
- Roux, A., Uyhazi, K., Frost, A. & De Camilli, P. GTP-dependent twisting of dynamin implicates constriction and tension in membrane fission. *Nature* **441**, 528–531 (2006).
- Freed, E. O. HIV-1 gag proteins: diverse functions in the virus life cycle. *Virology* **251**, 1–15 (1998).
- Greene, W. C. & Peterlin, B. M. Charting HIV's remarkable voyage through the cell: Basic science as a passport to future therapy. *Nature Med.* **8**, 673–680 (2002).
- Muller, B. *et al.* Construction and characterization of a fluorescently labeled infectious human immunodeficiency virus type 1 derivative. *J. Virol.* **78**, 10803–10813 (2004).
- Cramer, L. P. & Mitchison, T. J. Investigation of the mechanism of retraction of the cell margin and rearward flow of nodules during mitotic cell rounding. *Mol. Biol. Cell* **8**, 109–119 (1997).
- Mitchison, T. J. Actin based motility on retraction fibers in mitotic PtK2 cells. *Cell Motil. Cytoskel.* **22**, 135–151 (1992).
- Lehmann, M. J., Sherer, N. M., Marks, C. B., Pypaert, M. & Mothes, W. Actin- and myosin-driven movement of viruses along filopodia precedes their entry into cells. *J. Cell Biol.* **170**, 317–325 (2005).
- Mattapallil, J. J. *et al.* Massive infection and loss of memory CD4+ T cells in multiple tissues during acute SIV infection. *Nature* **434**, 1093–1097 (2005).
- Li, Q. *et al.* Peak SIV replication in resting memory CD4+ T cells depletes gut lamina propria CD4+ T cells. *Nature* **434**, 1148–1152 (2005).
- Favoreel, H. W., Van Minnebruggen, G., Adriaensen, D. & Nauwynck, H. J. Cytoskeletal rearrangements and cell extensions induced by the US3 kinase of an alphaherpesvirus are associated with enhanced spread. *Proc. Natl Acad. Sci. USA* **102**, 8990–8995 (2005).
- La Boissiere, S., Izeta, A., Malcomber, S. & O'Hare, P. Compartmentalization of VP16 in cells infected with recombinant herpes simplex virus expressing VP16-green fluorescent protein fusion proteins. *J. Virol.* **78**, 8002–8014 (2004).
- Huang, F., Khvorova, A., Marshall, W. & Sorkin, A. Analysis of clathrin-mediated endocytosis of epidermal growth factor receptor by RNA interference. *J. Biol. Chem.* **279**, 16657–16661 (2004).

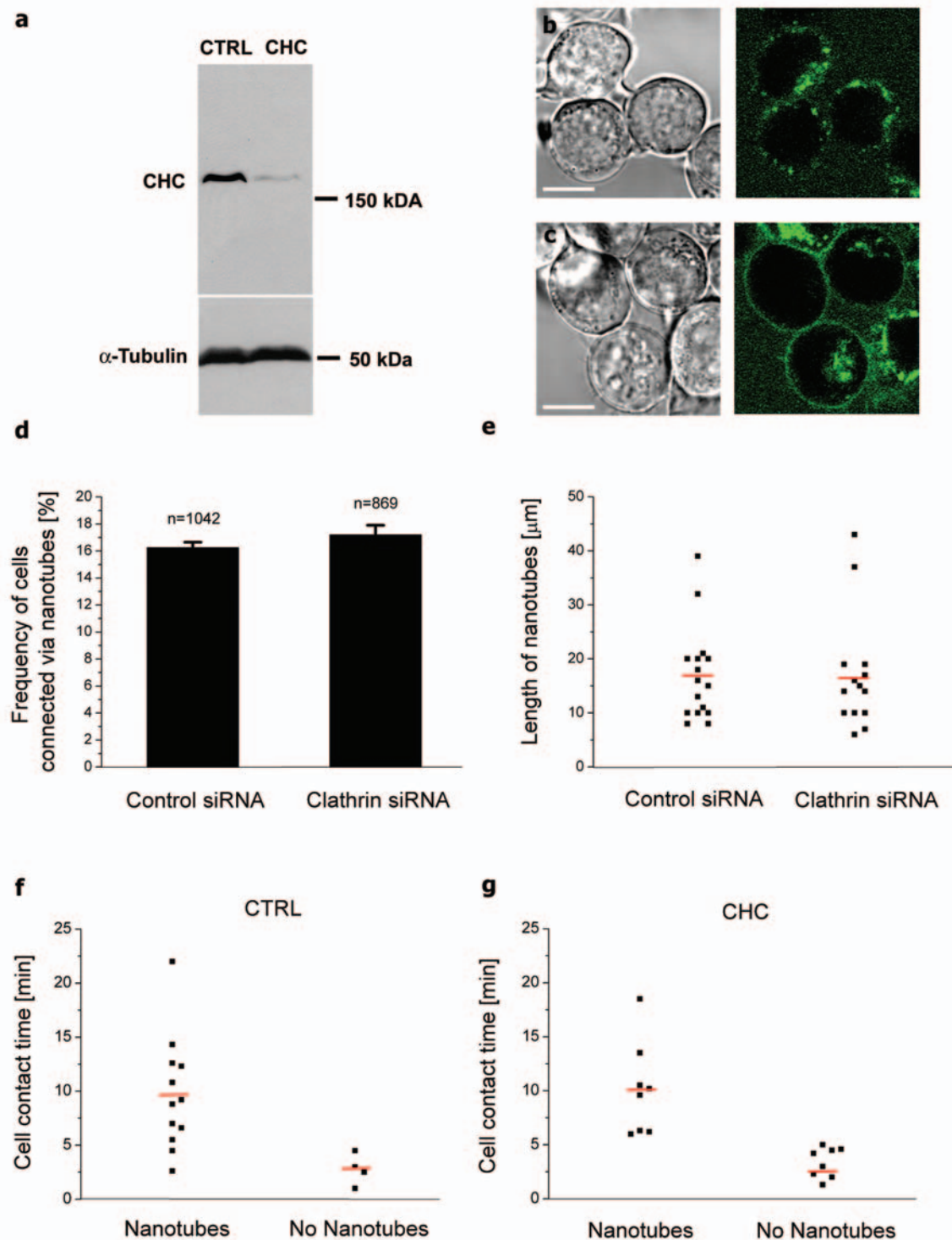


Figure S2 Efficient knockdown of clathrin heavy chain did not inhibit formation of T cell nanotubes. (a) Western blotting for clathrin heavy chain in lysates of Jurkat transfected with siRNA against clathrin heavy chain (CHC) or control siRNA (CTRL). Data are representative of four experiments. Jurkat cells transfected with (b) control siRNA or (c) siRNA against clathrin heavy chain were incubated with Alexa-488 transferrin and imaged by confocal microscopy. Clear surface staining of cells with clathrin knocked-down indicates a deficiency in their ability to efficiently internalize the fluorescent transferrin. Jurkat transfected with control siRNA or siRNA against clathrin heavy chain were incubated for 3 h on fibronectin-coated

slides and (d) the frequency of cells connected by nanotubes (n, number of cells counted over four independent experiments) or (e) the length of nanotubes (n=31), were measured. Differences between control and clathrin siRNA samples were not significant ($P > 0.4$). Time-lapse microscopy of (f) Jurkat T cells transfected with control siRNA (n=17) or (g) Jurkat T cells transfected with siRNA against clathrin heavy chain (n=16) was analyzed to record the length of time of contact between cells and then whether or not membrane nanotubes formed as cells departed. Contact between T cells led to nanotubes generally only after cells had been in contact for >4 min ($P < 0.01$, Mann-Whitney U).

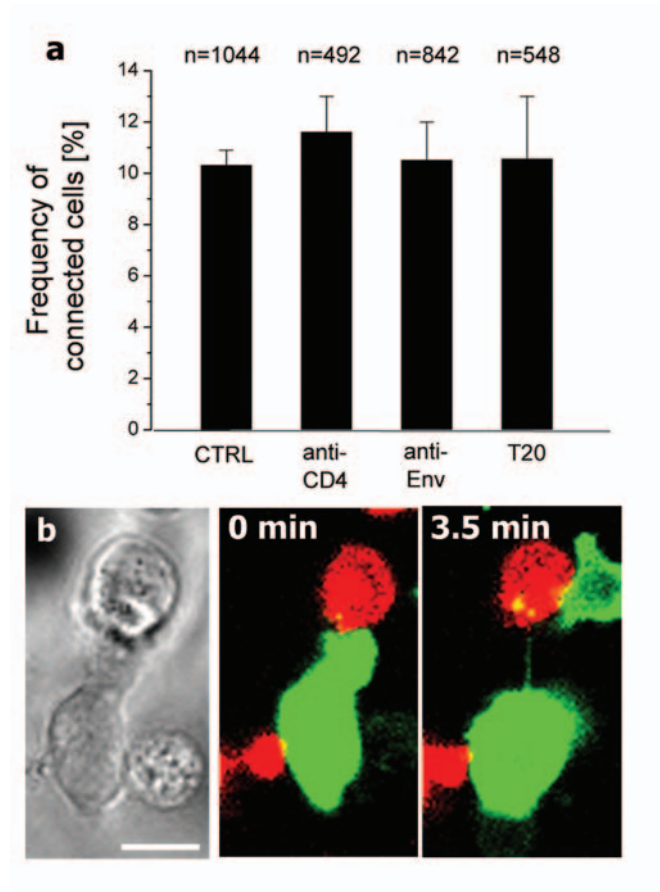


Figure S3: The frequency and formation of nanotubes between Jurkat_{LAI} is not influenced by the addition of mAb against CD4 or Env or the peptide inhibitor T20. (a) Jurkat_{LAI} were incubated with mAb or T20 and the frequency of cells being connected by nanotubes was scored. Differences were n.s. (b) In the

presence of T20, or mAb against CD4 or Env (data not shown), nanotubes were still seen to form after intercellular contact (n=8). Micrographs show uninfected Jurkat (labeled with DiO; green) and Jurkat_{LAI} (labeled with DiD; red). Data shown is representative of two independent experiments.

Supplementary movie legends

Movie S1 Rotation of a reconstructed 3D fluorescent image of a membrane nanotube connecting two Jurkat cells labeled with different membrane dyes. The movie shows that the nanotube does not lie on the substratum.

Movie S2 Time-lapse microscopy reveals the formation of membrane nanotubes between Jurkat T cells.

Movie S3 Unlabeled activated primary human T cells readily form membrane nanotubes after intercellular contact. Red dots indicate cells that become connected by a membrane nanotube.

Movie S4 Dynamic junctions in T cell nanotubes.

Movie S5 Serial sections through the membrane nanotube shown in Figures 4a and 4b

Movie S6 Serial sections through the membrane nanotube shown in Figures 4c and 4d.

Movie S7 Puncta of Gag-GFP (green) are clearly seen moving along a membrane nanotube that contains a junction highlighted by the uninfected cell being stained with a membrane dye DiD (red). Stills from this movie are shown in Fig. 5a.

Movie S8 A 3D reconstruction of 'optical slices' show that Gag-GFP (green) reaches the uninfected cell (red). One puncta of GFP remains close to the nanotube while another puncta of GFP has migrated away.